J Electr Eng Technol.2015; 10(3): 990-1001
http://dx.doi.org/10.5370/JEET.2015.10.3.990

ISSN(Print) 1975-0102
ISSN(Online) 2093-7423

Development of Analytical Models for Switched Reluctance Machine and their Validation

R. Jayapragash† and C. Chellamuthu*

Abstract – This paper presents analysis of Switched Reluctance Machine (SRM) using Geometry Based Analytical Model (GBAM), Finite Element Analysis (FEA) and Fourier Series Model (FSM) with curve fitting technique. Further a Transient Analysis (TA) technique is proposed to corroborate the analysis. The main aim of this paper is to give in depth procedure in developing a Geometry Based Analytical Model of Switched Reluctance Machine which is very accurate and simple. The GBAM is developed for the specifications obtained from the manufacturer and magnetizing characteristic of the material used for the construction. Precise values of the parameters like Magneto Motive Force (MMF), flux linkage, inductance and torque are obtained for various rotor positions taking into account the Fringing Effect (FE). The FEA model is developed using MagNet7.1.1 for the same machine geometry used in GBAM and the results are compared with GBAM. Further another analytical model called Fourier Series Model is developed to justify the accuracy of the results obtained by the methods GBAM and FEA model. A prototype of microcontroller based SRM drive system is constructed for validating the analysis and the results are reported.

Keywords: Switched Reluctance Machine (SRM), Geometry Based Analytic Model (GBAM), Fringing Effect (FE), Finite Element Analysis (FEA), Fourier Series Model (FSM) & Transient Analysis (TA)

1. Introduction

Besides being simple and robust, the absence of windings and magnets on the rotor in a Switched Reluctance Machine (SRM) makes it suitable for variable speed applications [1]. The SRM is highly non-linear in nature due to its doubly salient structure, magnetic characteristics and coupled relationship among rotor position, phase current and flux linkage [2]. As the linear model of the machine is unsuitable for high performance applications, various techniques are developed to incorporate the non-linearities in the machine.

Since the flux model proposed by A. Radun [3] could not be inverted to express stator current as a function of flux linkage and position, the model was found to be of little use further for real time implementation.

A non-linear analytical model of SRM based on the existing machine geometry and material properties using fourier series was presented by Ahmed Khalil et al [4, 5]. This model involved complex procedure and more information about the material.

Later, Wen Ding and Deliang Liang proposed a simple and rapid non-linear model of integrated SRS/G to characterize the inherent relationship among phase currents, rotor position, flux linkage and torque [6]. In this model, only the first five components of the Fourier Series describing the current in terms of arc tangent function are considered to express the whole flux linkage model $\psi(\theta,i)$ of SRS/G.

Analytical model of SRM considering mutual inductance was presented by D.N. Essah et al [7]. This model was developed by considering the mutual inductance between the phases alone. Comparison of different analytical models was done by Shoujun Song et al [8].

Non-linear modeling of SRM using Artificial Intelligence (AI) technique was addressed by T. Lachman et al [9]. The accuracy of the model developed using AI techniques mainly depends on the amount of the given flux linkage-current-position data and the prior number of fuzzy rules or the experimental knowledge.

Measurement of flux linkage and inductance of SRM using numerical integration technique reported by Rakesh Saxena et al [10] was proved to be laborious and relatively difficult to implement the control algorithms.

Huijun Zhou, Wen Ding and Zhenmin Yu reported a non-linear model of SRM using fourier series model [13]. To develop this model it is mandatory to use the data obtained either from FEA or from experimental set-up.

While analysis of SRM parameters using different methods have been reported in the past, the performance analysis of SRM considering saturation and fringing effect have not yet been discussed.

Though many methods were discussed for obtaining the inductance profile of the SRM, those techniques involved

† Corresponding Author: Dept. of Electrical and Electronics Engineering, St. Joseph's Institute of Technology, India. (r.jayapragash@gmail.com)
* Dept. of Electrical and Electronics Engineering, R.M.K. Engineering College, India. (malgudi60@hotmail.com)
Received: January 5, 2014; Accepted: December 2, 2014

complex computational procedures as well as requires data either from FEA model or from experimental set-up. It makes the steps involved more cumbersome and consumes more time for computation. More assumptions are made for analysis and model development, therefore accurate results may not be obtained.

In view of this, a Geometry Based Analytical Model (GBAM) is developed from machine geometry and magnetization characteristic of the material used by taking the fringing effect into account. Also a prototype SRM drive model is fabricated and the inductance profile is obtained using a simple technique called Transient Analysis (TA) technique.

This paper is organized into six sections. The various steps involved in developing the GBAM are discussed in section 2. While section 3 briefs the Finite Element Analysis (FEA) model of SRM, section 4 deals with comparison of both GBAM and FEA models. FSM development and its comparison with FEA model is discussed in Section 5. Section 6 explains the implementation of experimental model, results and validation.

2. Geometry Based Analytical Model of SRM

The detailed procedure for developing the GBAM is described below.

2.1 Calculation of aligned inductance

The inductance in a magnetic circuit is calculated using the expression

$$L = \frac{N^2}{R} \tag{1}$$

where N is the number of turns/pole

R is the summation of reluctances of different parts of the magnetic circuit.

Reluctance is expressed as

$$R = \frac{l}{(\mu A)} \tag{2}$$

where l is the length of the magnetic path

μ is the permeability of the medium

A is the cross sectional area of the flux path.

For air μ = 1.256e^{-6}, but for magnetic material it is not constant and depends on B and H.

Therefore expression for reluctance is expressed as

$$R = \frac{Hl}{BA} \tag{3}$$

where B is the flux density

H is the magnetic field intensity.

Values of B and H at each part of the machine are to be known to calculate their reluctances.

According to Ampere's circuital law,

$$MMF = NI = \sum (Hl) \tag{4}$$

Phase winding of the SRM is divided into two coils, with each coil having N turns placed on the diametrically opposite poles and carrying a current of I Amperes. Therefore the total MMF of the magnetic circuit is expressed as

$$MMF = 2NI \tag{5}$$

The flux path of the machine at the aligned position is shown in Fig. 1.

The path followed by the flux lines shown in Fig. 1 is considered for developing the equivalent magnetic circuit at the aligned position and it is shown in Fig. 2

Flux lines are closed lines and complete its path through stator yoke, stator pole, air gap, rotor pole and rotor yoke. Flux lines cross the stator pole, air gap and rotor pole twice. The equation to obtain total mmf in terms of magnetic field intensity (H) and length of the flux path (l) is expressed as

$$2NI = H_{sy}l_{sy} + 2H_{sp}l_{sp} + 2H_g l_g + 2H_{rp}l_{rp} + H_{ry}l_{ry} \tag{6}$$

where

H_{sy}, H_{sp}, H_g, H_{rp}, H_{ry} are the magnetic field intensities at

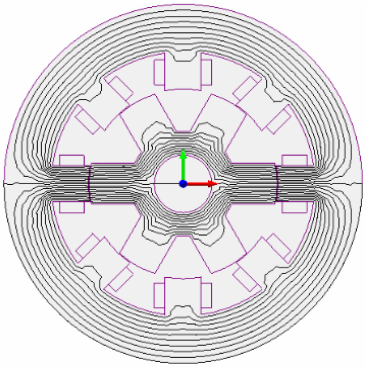

Fig. 1. Flux pattern at the aligned position

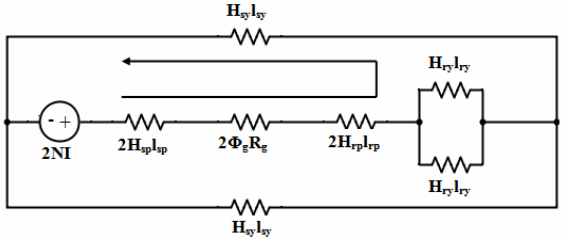

Fig. 2. Equivalent magnetic circuit at the aligned position

stator yoke, stator pole, air gap, rotor pole and rotor yoke respectively.

l_{sy}, l_{sp}, l_g, l_{rp}, l_{ry} are their corresponding lengths.

$$l_{sy} = \Pi\left(\frac{S_{yir} + S_{yor}}{2}\right) \quad (7)$$

where S_{yir}=Inner radius of stator yoke

S_{yor}=Outer radius of stator yoke

$$l_{sp} = S_{ph} \text{ ; Stator pole height} \quad (8)$$

$$l_{ry} = \Pi\left(\frac{R_{yir} + R_{yor}}{2}\right) \quad (9)$$

where R_{yir}=Inner radius of rotor yoke

R_{yor}=Outer radius of rotor yoke

$$l_{rp} = R_{ph} \text{ ; Rotor pole height} \quad (10)$$

The path of the air gap through which flux completes its path is a complex one and determining length of the air gap is difficult. As $H_g l_g = \Phi_g R_g$, instead of using $H_g l_g$ in the Eq. (6) $\Phi_g R_g$ is used where Φ_g is the flux through the air gap and R_g is the reluctance of the air gap. Procedure to obtain R_g is explained in section 2.2.

For air $\mu = 1.256e^{-6}$ is a constant. Therefore reluctance, $R = \frac{l}{(\mu A)}$ is found without the knowledge of B and H.

The new equation to calculate total mmf is expressed as

$$2NI = H_{sy} l_{sy} + 2H_{sp} l_{sp} + 2\phi_g R_g + 2H_{rp} l_{rp} + H_{ry} l_{ry} \quad (11)$$

Initially the net flux set up in the machine is assumed as low as $1e^{-8}$ and as this is the flux crossing the air gap, $\Phi_g = \Phi$. The flux carried by the different parts of the machine varies. Based on the amount of flux, the flux density at that part is calculated using the formula

$$B = \phi / A \quad (12)$$

Stator yoke carries only half the flux. Therefore flux density at stator yoke (B_{sy}) is represented as

$$B_{sy} = \left(\frac{\phi}{2A_{sy}}\right) \quad (13)$$

where A_{sy}= Area of stator yoke and it is given as

$$A_{sy} = S_{yt} * L \quad (14)$$

where S_{yt}=Stator yoke thickness

L=Stack length

Flux density at stator pole is expressed as

$$B_{sp} = \left(\frac{\phi}{A_{sp}}\right) \quad (15)$$

where A_{sp}= Area of stator pole and it is given as

$$A_{sp} = S_{pw} * L \quad (16)$$

where S_{pw}=Stator pole width

Rotor yoke carries only half the flux. Therefore flux density at rotor yoke (B_{ry}) is represented as

$$B_{ry} = \left(\frac{\phi}{2A_{ry}}\right) \quad (17)$$

Flux density at rotor pole is expressed as

$$B_{rp} = \left(\frac{\phi}{A_{rp}}\right) \quad (18)$$

where A_{rp}= Area of rotor pole and it is given as

$$A_{rp} = R_{pw} * L \quad (19)$$

where R_{pw}=Rotor pole width

For the known B, corresponding H is obtained by reverse mapping from the B-H data of M19 and it is shown in Fig. 3.

If the obtained B is greater than the data with us, it is limited to the maximum B. Thus H and l for different parts are obtained and $\Phi_g R_g$ is also known. Substituting these values in Eq. (11), left hand side value is compared with right hand side value. The flux is gradually increased till the error is less than 1%.

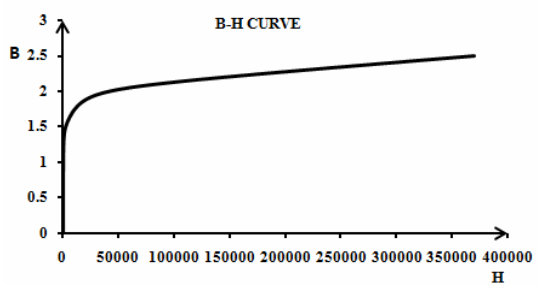

Fig. 3. B-H curve of M-19 steel

2.2 Air gap reluctance at the aligned position

The flux bulges in the air gap causing fringing effect and as the difference in the width of stator and rotor pole width is very small the boundary can be considered as circular with diameter equal to the air gap. Top view of the aligned position of stator and rotor pole is as shown in the Fig. 4.

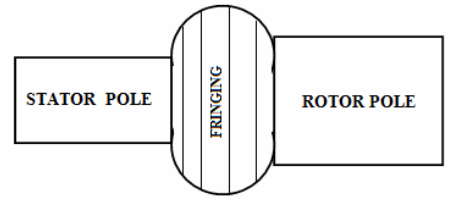

Fig. 4. Top view of the aligned position

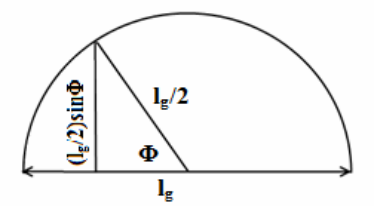

Fig. 5. Increment in the width

To calculate the air gap reluctance, the air gap is split into 100 vertical layers. The area of each layer gradually increases due to increase in the width and height of the air gap.

As shown in the Fig. 5, the increment in the width for any angle Φ will be (l_g/2) sinΦ. But two hemispherical regions are present so the total increment along the width or height of the air gap is $l_g$sinΦ. The total angle 180^0 is split into 100 partitions of 1.8^0 each.

$$\text{Length of individual layer} = \frac{l_g}{100}$$

Width of each layer = $w_m + l_g \sin\phi$, where w_m is mean of stator and rotor pole width.

$$\text{Height of each layer} = L + l_g \sin\phi \tag{20}$$

Area of the individual layer is the product of its width and height.

Reluctance of the individual layer is obtained using the Eq. (2). Total reluctance of the air gap R_g is summation of the reluctance of individual layer.

2.3 Reluctance calculation of iron parts

Reluctance of the Iron parts is calculated as follows.

Reluctance of stator yoke is given by

$$R_{sy} = \left(\frac{H_{sy} l_{sy}}{B_{sy} A_{sy}}\right) \tag{21}$$

Reluctance of stator pole is expressed as

$$R_{sp} = \left(\frac{H_{sp} l_{sp}}{B_{sp} A_{sp}}\right) \tag{22}$$

Reluctance of rotor pole is written as

$$R_{rp} = \left(\frac{H_{rp} l_{rp}}{B_{rp} A_{rp}}\right) \tag{23}$$

Reluctance of rotor yoke is

$$R_{ry} = \left(\frac{H_{ry} l_{ry}}{B_{ry} A_{ry}}\right) \tag{24}$$

Substituting the reluctance of various parts in the fundamental expression (1), the resultant expression to obtain reluctance as a function of current is given by

$$L_a(i) = \left(\frac{4NN}{2R_{sp} + 2R_g + 2R_{rp} + R_{ry} + R_{sy}}\right) \tag{25}$$

The result obtained by solving the Eq. (25) is shown in Fig. 6. The phase inductance is drooping when the current through the winding increases.

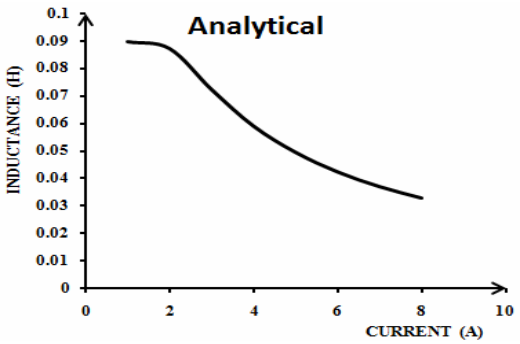

Fig. 6. Inductance Vs Current at aligned position

2.4 Calculation of unaligned inductance

The flux path of the machine in the unaligned position is shown in the Fig. 7.

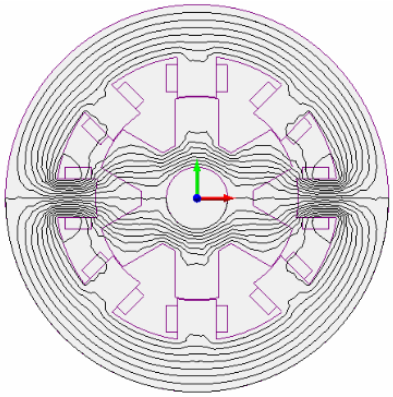

Fig. 7. Flux pattern at the unaligned position

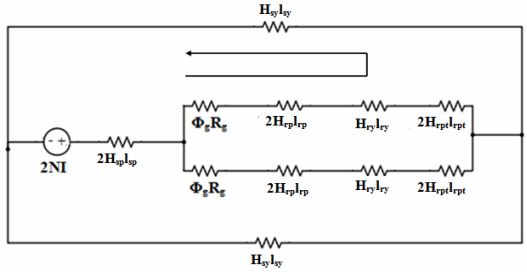

Fig. 8. Equivalent magnetic circuit at the un-aligned position

The path followed by the flux lines shown in Fig. 7 is considered for developing the equivalent magnetic circuit at the unaligned position and it is shown in Fig. 8.

Equation to obtain total mmf of the magnetic path shown in the equivalent circuit is given as

$$2NI = 2H_{sp}l_{sp} + \phi_g R_g + 2H_{rp}l_{rp} + H_{ry}l_{ry} + 2H_{rpt}l_{rpt} + H_{sy}l_{sy} \quad (26)$$

where H_{rpt}=Magnetic field intensity at the rotor pole tip
l_{rpt}=Length of the rotor pole tip

2.5 Air gap reluctance at the un-aligned position

The flux lines crossing the air gap at unaligned position is given in detail in the Fig. 9. Based on symmetry only half of the total flux is considered for analysis. The air gap is treated as combination of three sections as shown in the Fig. 9. The sections can be treated as ideal geometrical figures without much loss in accuracy.

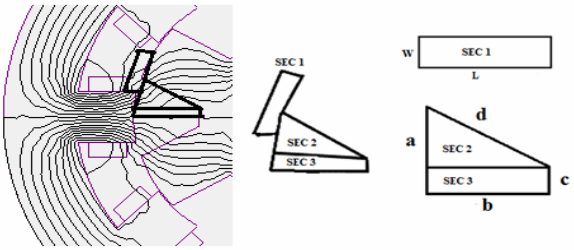

Fig. 9. Different sections of the air gap at unaligned position

Section 1 – It is modeled as a rectangle, with length equal to the distance between the stator pole tip and the centre of the rotor pole. The centre of rotor pole is at an angle 30 deg from the horizontal and the stator pole tip is at an angle half of the stator pole arc. Considering rotor pole radius as a common radius the length is found using the formula, Arc length = Radius * Arc angle. Divergence of flux lines at the stator pole tip is generally limited to 2mm. Therefore the width is (l_g+2mm). Reluctance of the section 1 is computed as follows.

Length of the air gap is given as

$$l = R_{pr}(30 - S_{arc}/2)\frac{\Pi}{180} \quad (27)$$

where R_{pr}=Rotor pole radius
S_{arc}=Stator pole arc

Area of the air gap is expressed as

$$A = W * L \quad (28)$$

where

$$W = \text{width of the air gap} = l_g + 2mm \quad (29)$$

Reluctance of section 1 is described as

$$R_1 = \frac{l}{(4\pi e^{-7} * A)} \quad (30)$$

The sides of the Fig. 9 are a, b, c and d which are given as a - distance from centre of stator pole to rotor pole tip, it is expressed as

$$a = R_{pr}(30 - R_{arc}/2)\frac{\Pi}{180} \quad (31)$$

b and d - distance between rotor yoke and stator pole tip, it is written as

$$b = d = R_{ph} + l_g \quad (32)$$

where R_{ph}=Rotor pole height
c - half the distance between two rotor poles, it is given as

$$c = \left(2\Pi R_{yor} - 6R_{pw}\right)/12 \quad (33)$$

Section 2 – It has 3 sides, which are a-c, b and d.

Section 2 is separated in to 100 horizontal layers of uniform area and varying length.

Length of each layer= $nb/100$, where n=1 to 100

Area of each layer = $(a-c)L/100$

Reluctance of each layer is calculated and the reluctance of section 2 (R_2) is parallel combination of hundred layers.

Section 3 – It has sides 'b' and 'c' and reluctance of this section is described as

$$R_3 = \left(\frac{b}{\{4\Pi e^{-7}[c * L]\}}\right) \quad (34)$$

Reluctance of 3 sections is in parallel and the total air gap reluctance is given as

$$R_g = \left(\frac{1}{\left\{\left(\frac{1}{R_1}\right) + \left(\frac{1}{R_2}\right) + \left(\frac{1}{R_3}\right)\right\}}\right) \quad (35)$$

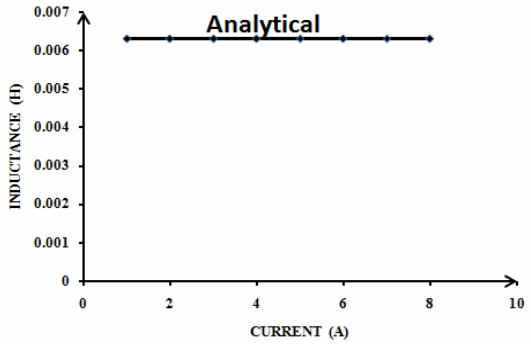

Fig.10. Inductance Vs Current at un-aligned position

The variation of unaligned inductance for the change in current value is very minimum. Therefore it is considered as constant value for particular SRG and it is expressed as

$$L_u = \left(\frac{4NN}{\left(2R_{sp} + 2R_g + 2R_{rp} + R_{ry} + 2R_{rpt} + R_{sy}\right)} \right) \tag{36}$$

The result obtained by solving Eq. (36) is given in Fig. 10.

2.6 Inductance profile of SRM

The phase inductance is drooping when the rotor leaves the aligned position. During falling inductance period, variation of inductance with respect to rotor position is negative. Therefore torque generated is also negative [11]. If the phase is excited in this period, rotor experiences torque which opposes rotation and extracts energy from the turbine. Inductance variation as a function of current and position is given as

$$L(I,\theta) = a_0(i) + a_1(i)\cos N_r\theta \tag{37}$$

where

$$a_0(i) = \frac{1}{2}\left(L_a(i) + L_u\right) \tag{38}$$

$$a_1(i) = \frac{1}{2}\left(L_a(i) - L_u\right) \tag{39}$$

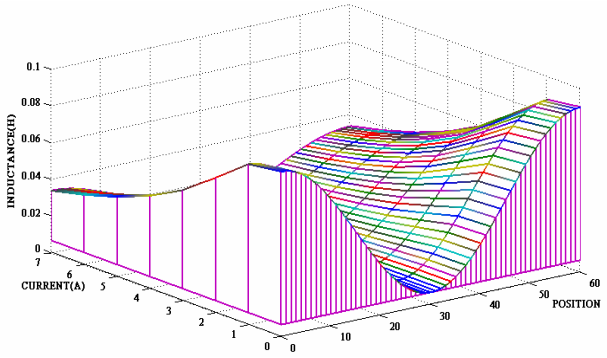

Fig. 11. Inductance variation as a function of current and position

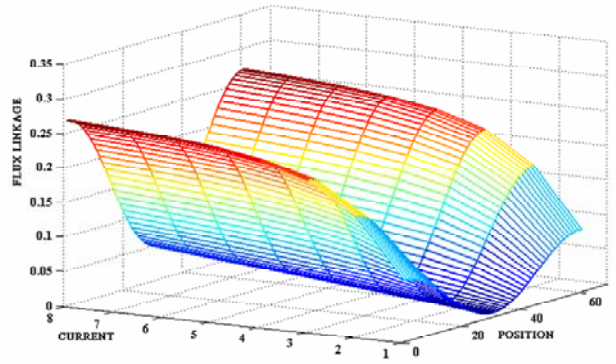

Fig. 12. ψ-i characteristics of SRM

Complete cycle of inductance variation as a function of current and position is shown in Fig. 11.

2.7 Flux linkage calculation

Flux linkage as a function of current and position is expressed as

$$\psi(I,\theta) = L(I,\theta)I \tag{40}$$

Fig. 12 shows ψ-i characteristics of SRM where it is evident that a nonlinearity exists at the aligned position and is considered by making the fourier series coefficients $a_o(i)$ and $a_1(i)$ dependent on the phase current.

2.8 Torque calculation

The instantaneous torque as a function of current and position is calculated using the formula

$$T(I,\theta) = \frac{1}{2}I^2\frac{dL(I,\theta)}{d\theta} \tag{41}$$

The response obtained by solving the Eq. (41) is given in Fig. 13. During falling inductance period, variation of inductance with respect to rotor position is negative. Therefore torque generated is also negative.

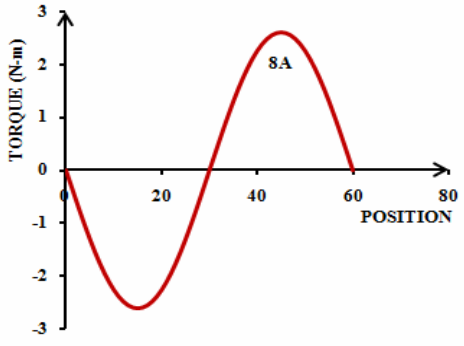

Fig. 13. Torque Characteristics

3. FEA Model

Among various numerical methods FEA is most frequently used. There are many types of software available to analyze and compute the electromagnetic field of the machine accurately in two-dimension (2-D). In this paper MagNet 7.1.1 is used to build the model. The FEA model of 4 Phase 8/6 SRM is shown in Fig. 14 (a) for the specifications in Table 4.

The mesh pattern of the problem region at the aligned and unaligned positions is shown in Fig. 14 (b) and Fig. 14 (c) respectively.

FEA Model shown in Fig.14 is solved to obtain the data like flux linkage, inductance and torque. The variation of flux linkage with respect to current is shown in Fig. 15.

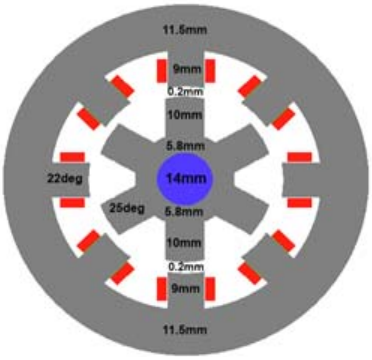

(a)

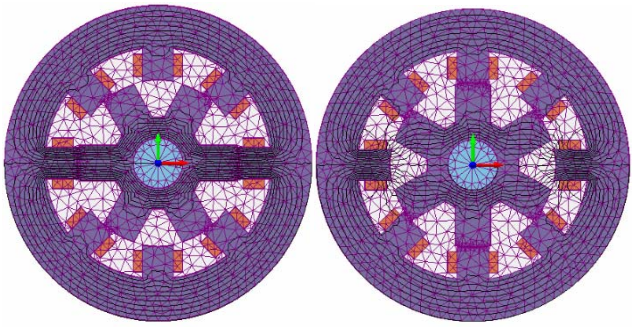

(b) (c)

Fig. 14. (a) FEA Model of 4 Phase 8/6 SRG; (b) and (c) Mesh pattern at aligned and un- aligned positions

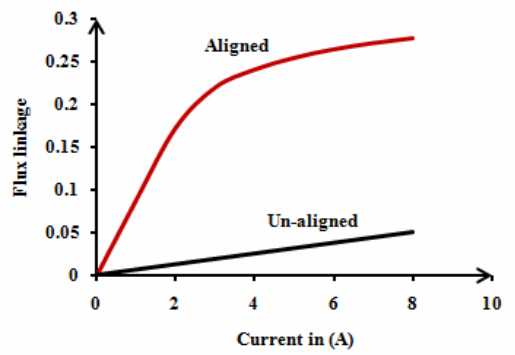

Fig. 15. Flux Linkage vs Current

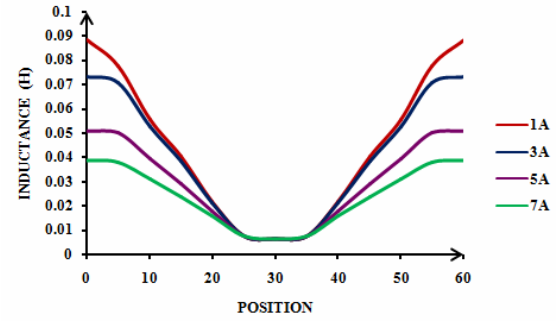

Fig. 16. Inductance Profile

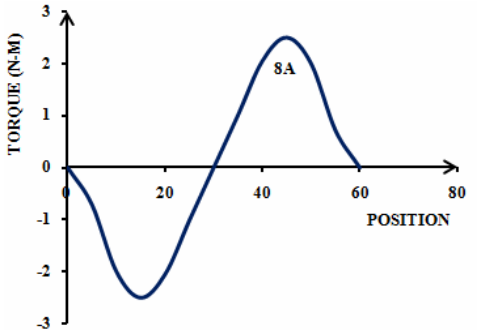

Fig. 17. Torque characteristics

It is evident from Fig. 16 that inductance is maximum at the aligned position. When the rotor leaves the aligned position inductance decreases and it is minimum at the unaligned position. The inductance profile of the machine is periodic function of rotor position as seen in Fig. 16.

Torque obtained from FEA model for various values of current and position is shown in Fig. 17. It is negative from 0-30 degrees and positive from 30-60 degrees.

4. Comparison of Analytical Model with FEA Model

The response of flux model is compared with ψ-i characteristics of FEA model and is shown in Fig. 18. The comparison is done at aligned and unaligned positions. The results indicate there exists a close match between analytical model and FEA model.

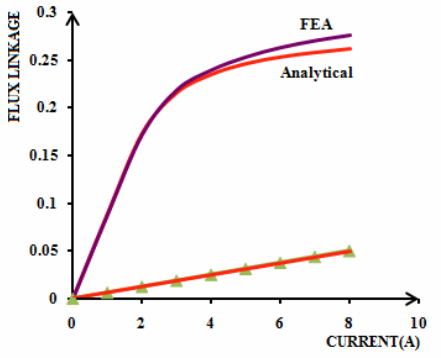

Fig. 18. Flux linkage comparison with FEA

The inductance profile obtained from analytical model is compared with FEA model for a fixed value of current and is shown in Fig. 19. This result also reveals that the Analytical Model and FEA model are alike.

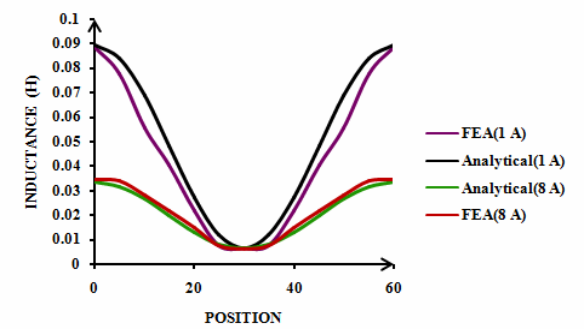

Fig. 19. Inductance comparison with FEA

Comparison of the torque obtained from Analytical model is performed with FEA and is shown in Fig. 20.

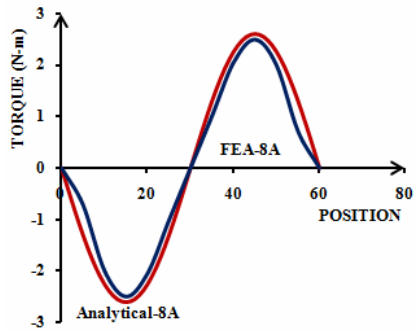

Fig. 20. Torque comparison with FEA

5. Fourier Series Model of SRM

The nonlinear model to SRM in terms of fourier series expression of phase self-inductance is calculated analytically, under the assumption of negligible mutual effect between the individual SRM phases and various losses. A fourier series representation is used to express the phase inductance with respect to the rotor position as [13]

$$L(\theta,i) = L_0(i) + \sum_{n=1}^{\infty} L_n(i)\cos(nN_r\theta) \tag{42}$$

where

$L(\theta,i)$ – phase inductance
$L_0(i)$ & $L_n(i)$ – fourier series co-efficients
N_r – number of rotor poles
θ – angular position of the rotor

To determine the coefficients in the Fourier series, it is necessary to know the inductance at several specific positions. The following relevant assumptions are further made for an 8/6 SRM:

$L_a(i) = L(0,i)$ - aligned inductance
$L_i(i) = L(10,i)$ – one third way inductance
$L_m(i) = L(15,i)$ – mid way inductance
$L_j(i) = L(20,i)$ – two third way inductance
$L_u(i) = L(30,i)$ – un-aligned inductance

The general expression of inductance considering the five different positions as stated above is approximated as

$$L(\theta,i) = L_0(i) + \sum_{n=1}^{4} L_n(i)\cos(nN_r\theta) \tag{43}$$

where

$$L_0(i) = \frac{1}{6}L_a(i) + \frac{1}{3}L_i(i) + \frac{1}{3}L_j(i) + \frac{1}{6}L_u(i) \tag{44}$$

$$L_1(i) = \frac{1}{3}L_a(i) + \frac{1}{3}L_i(i) - \frac{1}{3}L_j(i) - \frac{1}{3}L_u(i) \tag{45}$$

$$L_2(i) = \frac{1}{4}L_a(i) - \frac{1}{2}L_m(i) + \frac{1}{4}L_u(i) \tag{46}$$

$$L_3(i) = \frac{1}{6}L_a(i) - \frac{1}{3}L_i(i) + \frac{1}{3}L_j(i) - \frac{1}{6}L_u(i) \tag{47}$$

$$L_4(i) = \frac{1}{12}L_a(i) - \frac{1}{3}L_i(i) + \frac{1}{2}L_m(i) - \frac{1}{3}L_j(i) + \frac{1}{12}L_u(i) \tag{48}$$

For different values of current i, $L_a(i)$, $L_i(i)$, $L_m(i)$, $L_j(i)$ and $L_u(i)$ are calculated using the data obtained from either FEA method or experimental measurement and it is shown in Fig. 21.

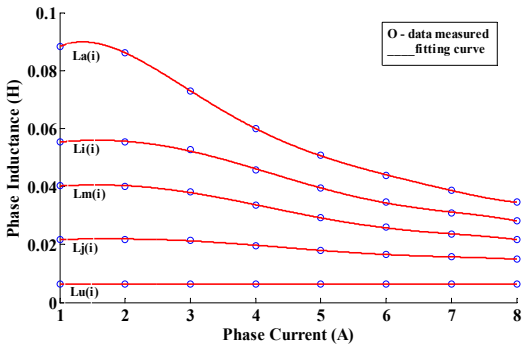

Fig. 21. Inductance and fitting curve

The generalized equation for $L_a(i)$, $L_i(i)$, $L_m(i)$, $L_j(i)$ and $L_u(i)$ are obtained using curve fitting technique. Which are expressed as follows

$$L_a(i) = 2.6401e{-}005x^5 - 0.00070554x^4 + 0.0071701x^3 - 0.033227x^2 + 0.057112x + 0.057889 \tag{49}$$

$$L_i(i) = -1.0535e{-}005x^5 + 0.00020576x^4 - 0.0012112x^3 + 0.0012507x^2 + 0.0022113x + 0.052899 \tag{50}$$

$$L_m(i) = -6.8952e\text{-}006x^5 + 0.00013258x^4 - 0.0007485x^3 + 0.00051689x^2 + 0.002069x + 0.038168 \quad (51)$$

$$L_j(i) = -4.4635e{-}006x^5 + 9.4517e{-}005x^4 - 0.00067528x^3 + 0.0017303x^2 - 0.0016665x + 0.022309 \quad (52)$$

$$L_j(i) = 6.7307e{-}021x^5 - 1.8665e{-}019x^4 + 1.9187e{-}018x^3 - 9.012e{-}018x^2 + 1.8969e{-}017x + 0.006209 \quad (53)$$

The inductance profile obtained using curve fitting technique for various values of current is compared with FEA model and it is shown in Fig. 22.

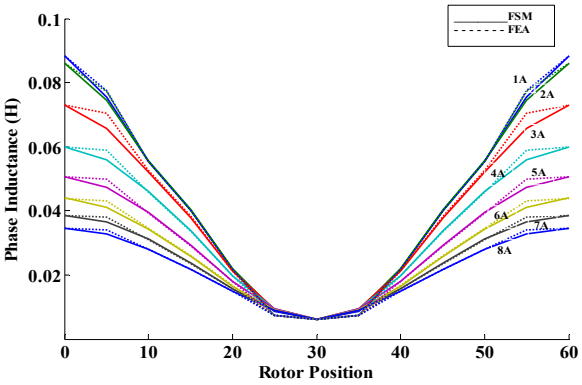

Fig. 22. Inductance comparison

As per non-linear inductance model, the torque is described as

$$T(\theta,i) = (-N_r)\sum_{n=1}^{4}\left[n.\sin(nN_r\theta).\int_0^i i.L_n di \right] \quad (54)$$

The above equation is solved to obtain the torque response of the SRM and it is given in Fig. 23.

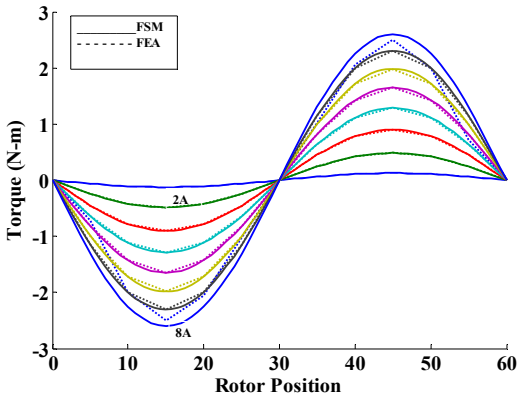

Fig. 23. Torque comparison

From the results it is clear that the fourier series model is accurate but it cannot be developed without using the data obtained either from FEA model or from experiments measurement. Many number of data are assumed for analysis and model development. Therefore, GBAM is developed and discussed in detailed manner.

6. Experimental Results

The Parameters like inductance, flux linkage and torque obtained from AM is confirmed with FEA model and found that there is a close match between the parameters. Hardware model [12] is developed to validate the inductance at the aligned and un aligned positions The complete block diagram of the experimental set up is shown in Fig. 24.

For validation of the inductance values, microcontroller based experimental set up is developed and it is shown in Fig. 25. The stator winding of the SRM is excited by DC supply obtained from a full bridge diode rectifier powered by an Auto-Transformer. MOSFET IRF540 and 1 ohm resistor are connected in series with the phase winding. Triggering signal required for the MOSFET is generated by ATMEGA16 microcontroller and it is supplied to the gate terminal of the MOSFET through Opto-isolator MCT2E.

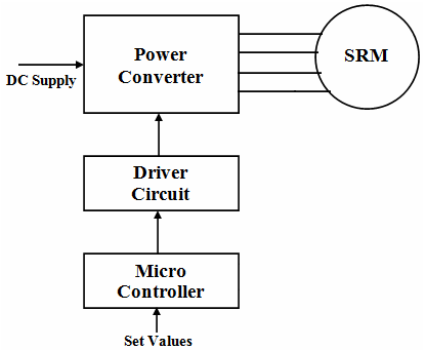

Fig.24. Block diagram of the experimental set up

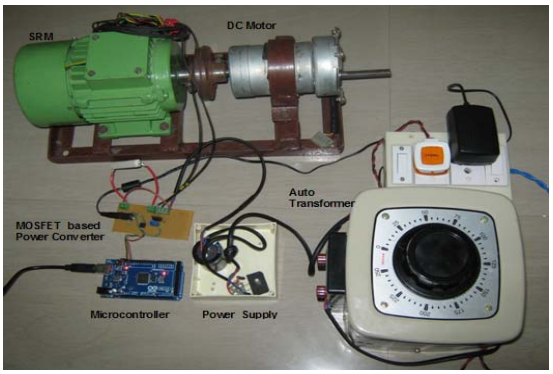

Fig. 25. Experimental set up

Power circuit for energizing one of the phase winding through MOSFET IRF540 is shown in Fig. 26.

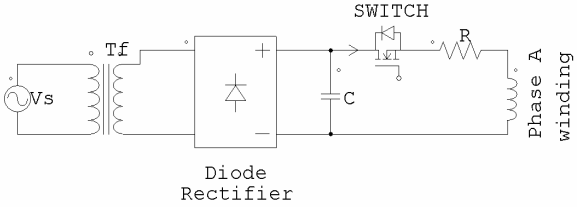

Fig. 26. Power Circuit

Gate signal is obtained from microcontroller and it is supplied to the gate terminal of the MOSFET through driver circuit. The complete circuit diagram of the driver circuit is shown in Fig. 27.

One of the phase winding is excited to bring the rotor to aligned position. Voltage applied to the stator winding is varied to adjust the current flow through the winding and transient response is captured using Digital Storage Oscilloscope (DSO). From the rise time of the transient response, inductance is obtained at aligned position for various values of current. Electrical equivalent circuit of the phase winding is shown in Fig. 28.

The voltage equation corresponding to electrical equivalent of the phase winding for zero initial current [i(0)=0] is expressed as

$$V = L(i,\theta)\frac{di}{dt} + iR \tag{55}$$

Solving the non-linear Eq. (42) gives the result as

$$i(t) = \frac{V}{R}(1 - e^{\frac{-t}{\tau}}) \tag{56}$$

where

$$\tau = \frac{L}{R} \tag{57}$$

When t=5τ, system reaches steady state and inductance value is obtained from the rise time of the transient response. Transient response of the drive system when the winding carries 1A and 2A are shown in Fig. 29 and Fig. 30 respectively.

From the transient characteristic of the real time system

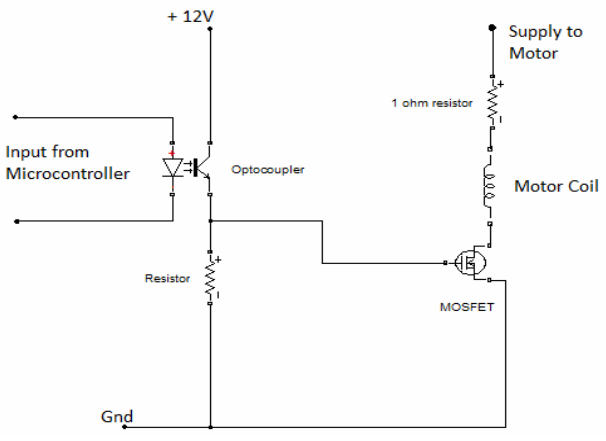

Fig. 27. Driver Circuit

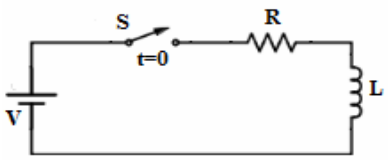

Fig. 28. Electrical equivalent of phase winding

inductance is obtained for the various values of current and it is compared with the FEA model and Analytical model. The results are tabulated in Table 1.

Flux linkage at the aligned position for different values of current is calculated from inductance obtained from experimental set up and it is compared with the FEA model and Analytical model. The results are tabulated in Table 2.

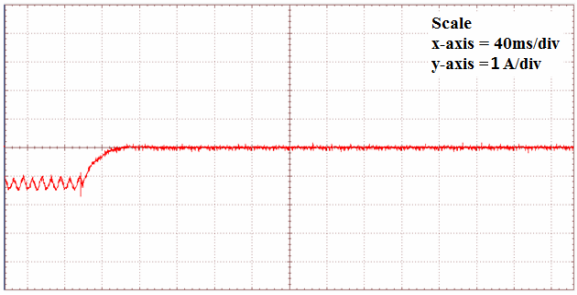

Fig. 29. Transient current characteristic at 1A

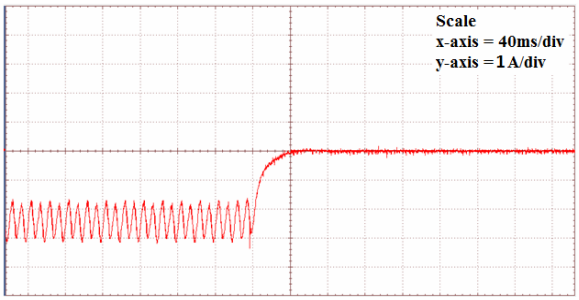

Fig. 30. Transient current characteristic at 2A

Table 1. Inductance value comparison at aligned position

Current (A)	GBAM Model (H)	FEA Model (H)	Experimental Result (H)
1	0.089549	0.088258	0.087
2	0.087039	0.086151	0.086
3	0.072164	0.073012	0.071
4	0.058908	0.059966	0.057
5	0.049397	0.050716	0.048
6	0.042325	0.043907	0.041
7	0.036961	0.038678	0.035
8	0.032815	0.034548	0.031

Table 2. Flux linkage comparison at aligned position

Current (A)	GBAM Model	FEA Model	Experimental Result
1	0.089549	0.088258	0.087
2	0.174078	0.172302	0.172
3	0.216492	0.219036	0.213
4	0.235632	0.239864	0.228
5	0.246985	0.25358	0.24
6	0.25395	0.263442	0.246
7	0.258727	0.270746	0.245
8	0.26252	0.276384	0.248

Table 3. Inductance value comparison at un-aligned position

GBAM Model (H)	FEA Model (H)	Experimental Result (H)
0.0062	0.0062	0.0062

Un-aligned position is obtained by exciting two phase windings simultaneously and un-aligned inductance is obtained for various values of current. It is found that un-aligned inductance is constant irrespective of the current magnitude and it is shown in Table 3.

7. Conclusion

The Geometry Based Analytical Model of SRM considering fringing effect is discussed briefly and the results are compared with the FEA model of a SRM. The results show that a close matches between analytical and FEA models exist. The analytical model presented is very accurate, simple and it consumes less time than the other methods and also gives results close to FEA. Further for justifying the results obtained from GBAM another analytical method called Fourier Series Model is developed with curve fitting technique. The results obtained from FSM is verified with the FEA and found satisfactory but it is mandatory to use the data obtained either from FEA model or from experimental measurements. Many numbers of data are assumed for analysis and model development. Therefore, GBAM is developed and it does not require any data from FEA model/experimental measurements. Implemented microcontroller based SRM drive system comprises of SRM has the same machine geometry which is considered for analytical model. Inductance profile of the machine is obtained for various values of current using Transient Analysis Technique and it is validated with the analytical and FEA models.

Annexure

Table 4. Electrical specifications of SRM

Rated Power	1Hp (746w)
Rated Speed	3000 RPM
Rated Voltage	330 V,DC
Rated Current	5 A

Construction and mechanical specifications

Winding gauge	24 SWG
No. of turns per pole	100 turns
Stator core stamping thickness	0.5 mm
Rotor core stamping thickness	0.5 mm
Shaft diameter	14 mm
Thickness of rotor yoke	5.8 mm
Height of rotor pole	10 mm
Air gap length	0.2 mm
Height of stator pole	9 mm
Thickness of stator yoke	11.5 mm
Stack length	80 mm
Stator pole arc	22 deg
Rotor pole arc	25 deg
Material used CRNGO grade M-19	

References

[1] T.J.E. Miller, "Switched reluctance motors and their control," Oxford University Press, 1993.

[2] R. Krishnan, "Switched reluctance motor drives, modeling, simulation, analysis, design and applications," CRC Press, 2001.

[3] A. Radun, "Analytical calculation of switched reluctance motor's unaligned inductance," IEEE Trans. Magn., vol. 35, No. 6, pp. 4473-4481, Nov. 1999.

[4] S. A. Hossain and I. Husain, "A geometry based simplified analytical model of switched reluctance machines for real-time controller implementation," IEEE Trans. Power Electron., vol. 18, No. 6, pp. 1384-1389, Nov. 2003.

[5] Ahmed Khalil and I. Husain, "A Fourier Series Generalized Geometry-Based Analytical Model of Switched Reluctance Machines," IEEE Trans. Ind. Applications, vol. 43, No. 3, pp. 673-684, June 2007.

[6] Wen Ding and Deliang Liang, "A Fast Analytical Model for an Integrated Switched Reluctance Starter/ Generator," IEEE Trans. Energy Conversion, vol. 25, No. 4, pp. 948-956, Dec 2010.

[7] D.N. Essah and S.D. Sudhoff, "An Improved Analytical Model for the Switched Reluctance Motor," IEEE Trans. Energy Conversion, vol. 18, No.3, pp. 349-356, Sep 2003.

[8] Shoujun Song and Weiguo Liu, "A Comparative Study on Modeling Methods for Switched Reluctance Machines," Computer and Information Science, vol. 03, No.02, pp. 205-210, May 2010.

[9] T. Lachman, T. R. Mohamad, and C. H. Fong, "Non-linear modeling of switched reluctance motors using artificial intelligence techniques," IEE Procs-Elec Power Appl, vol. 151, no. 1, pp. 53-60, Jan. 2004.

[10] Rakesh Saxena, Bhim Singh and Yogesh Pahariya, "Measurement of flux linkage and inductance profile of SRM" International Journal of Computer and Electrical Engineering, Vol. 2, No. 2, April 2010.

[11] David A. Torrey, "Switched reluctance generators and their control," IEEE Transactions on Industrial Electronics, Vol.49, No.1, Feb 2002.

[12] Yuan-Chih, Chang-Ming Liaw, "On the design of power circuit and control scheme for switched reluctance generator," IEEE Transactions on Power Electronics, Vol. 23, No.1, January 2008.

[13] Huijun Zhou, Wen Ding and Zhenmin Yu, "A non-linear model for the switched reluctance motor," School of Electrical Engineering, Xi'an 710049, China, 568-571.

[14] Help Browser of MagNet7.1.1, Infolytica Corporation

R. Jayapragash He received the A.M.I.E. degree in Electrical Engineering from Institution of Engineers (India), Kolkatta in 2004 and M.E. degree in Power Electronics and Drives from A.C. College of Engineering and Technology, Anna University, Tamil Nadu in 2007. He is presently pursuing Ph.D in Anna University, Chennai, India. He is currently an Associate Professor in the Department of Electrical and Electronics Engineering, St. Joseph's Institute of Technology, Chennai, India. His research interests are Analytical Model Development, Control of Electrical Drives and Renewable Energy Systems.

C. Chellamuthu He received Ph.D degree in Power Electronics from IIT Chennai, India. He is currently working as a Professor in the department of Electrical and Electronics Engineering, R.M.K. Engineering College, chennai, India. His area of interests are Power Electronics, Electrical Drives and Control, Microprocessor based System Design, Networking and Image Processing.